Available online at www.sciencedirect.com

jmr&t
Journal of Materials Research and Technology

journal homepage: www.elsevier.com/locate/jmrt

Effect of pore structure on the thermal stability of shape-stabilized phase change materials

Soumen Mandal [a,1], *Shafiq Ishak* [b,c,1], *Mohd Azreen Mohd Ariffin* [d], *Dong-Eun Lee* [e,*], *Taejoon Park* [f,**]

[a] *Intelligent Construction Automation Center, Kyungpook National University, 80, Daehakro, Buk-gu, Daegu 41566, South Korea*
[b] *Department of Structure and Materials, Faculty of Civil Engineering, University of Technology Malaysia (UTM), Johor Bahru, 81310, Johor, Malaysia*
[c] *Department of Architectural Engineering, Hanyang University, 1271 Sa 3- dong, Sangnok-gu, Ansan-si, 15588, South Korea*
[d] *Forensic Engineering Centre (FEC), Institute of Smart Infrastructure and Innovative Construction (ISIIC), School of Civil Engineering, Faculty of Engineering, Universiti Teknologi Malaysia, 81310 Johor Bahru, Johor, Malaysia*
[e] *School of Architecture, Civil, Environment, and Energy, Kyungpook National University, 1370, Sangyegk-Dong, Buk-Gu, Daegu 702701, South Korea*
[f] *Department of Robotics Engineering, Hanyang University, 55 Hanyangdaehak-ro, Ansan, Gyeonggi-do 15588, South Korea*

ARTICLE INFO

Article history:
Received 1 February 2023
Accepted 24 May 2023
Available online 27 May 2023

Keywords:
Biochar
Enthalpy
Thermal energy storage
Phase change material
Composite

ABSTRACT

To attain the increasing demand for energy in addition with an aim of resolving environmental concerns, a transition from traditional energy systems to renewable resources is crucial. However, renewable energy needs the proper mechanism of harvesting on availability and suitable storage capabilities until it's utilizable necessity. Therefore, effective and consistent energy storage frameworks are crucial for the utilization of stowed renewable energy at a maximum capacity. Pondering that, this study has been focused on the utilization of biochars for efficacious thermal energy storage applications. The shape stabilization efficiency of commercial softwood biochar (EB) has been compared with synthesized bamboo biochar (BA). Both biochars have demonstrated porous and channel-like morphologies and the BET surface areas are measured to be 41.1676 and 9.7213 m^2/g, respectively. Paraffin as a phase change material (PCM) is melted and permeated into the biochars to synthesize the biochar composite PCMs. Paraffin to biochar in a 3:1 ratio has been realized as the optimum for both composite PCMs. Maximum heat charging and discharging enthalpies are found to be 96.71 and 94.97 J/g for 1:3 EB-PCM as well as 77.78 and 75.06 J/g for 1:3 BA-PCM composites, respectively. The highest encapsulation ratios are calculated to be 53.49 and 43.02% for 1:3 EB-PCM and 1:3 BA-PCM composites, respectively. Although the enthalpies and encapsulation ratios are found higher in EB-PCM composites, BA-PCM composites have demonstrated superior thermal stability owing to the smaller pore sizes and that has resulted in higher surface tension, capillary action, and effective surface functionalities.

* Corresponding author.
** Corresponding author.
E-mail addresses: dolee@knu.ac.kr (D.-E. Lee), taejoon@hanyang.ac.kr (T. Park).
[1] Authors have contributed equally.

https://doi.org/10.1016/j.jmrt.2023.05.217

Abbreviations

TES	Thermal energy storage
EB	Commercial softwood biochar
BA	Bamboo biochar
PCM	Phase change material
PRBA	Paraffin permeated into bamboo biochar
PREB	Paraffin permeated into commercial softwood biochar
GHG	Greenhouse gas
FE-SEM	field emission scanning electron microscope
BET	Brunauer, Emmett, Teller
BJH	Barrett- Joyner-Halenda
ATR-FTIR	Attenuated total reflectance-Fourier-transform infrared
TG/DTA	Simultaneous thermogravimetric/ differential thermal analyzer
TGA	Thermogravimetric analysis
DTG	Differential thermogravimetric analysis
DSC	Differential scanning calorimeter
IUPAC	International Union of Pure and Applied Chemistry
N_2	Nitrogen
Å	Angstrom
°C	Degree Celsius
J/g	Joule per gram
T_m	Melting temperature
T_s	Solidification temperature
ΔH_m	Melting enthalpy
ΔH_s	Solidification enthalpy
EE%	Encapsulation efficiency
ER%	Encapsulation ratio
$\Delta H_{m,\ Composite\ PCM}$	Melting enthalpy of biochar PCM composites
$\Delta H_{s,\ Composite\ PCM}$	Solidification enthalpy of biochar PCM composites
$\Delta H_{m,\ Paraffin}$	Melting enthalpy of paraffin
$\Delta H_{s,\ Paraffin}$	Solidification enthalpy of paraffin
$-COO^-$	Carboxylate group
$-OH^-$	Hydroxy group
-CO	Carbonyl group
-R-OH	Alcohols
$-NH_2$	Amino group
π-electron	Pi electron
h	hours
min	Minutes
STP	Standard temperature and pressure
cm	Centimeter
cm^3/g	Gram per cubic centimeter

1. Introduction

Greenhouse gases (GHGs) cause global temperature to rise by trapping solar energy. Since the very beginning of the industrial revolution, GHGs from fossil fuel burning have been causing global warming and it has reached an alarming stage with the increasing demand of their uses. Transportation is one of the major sectors responsible for a quarter of entire GHG emanations, owing to the major dependency on fossil-fuel based vehicles [1]. Besides the emissions from fossil fuels, approximately 40% of greenhouse gas emissions are instigated by the construction industries [2]. Therefore, renewable energy might bring the most suitable solutions for alternative energy resources and can circumvent environmental contaminations. Thus, research on renewable energy has attracted tremendous attention globally with the use of natural energy sources, which can keep an impact on the environment and society [3]. Emerging new energy resources is crucial with the comprehension of suitable energy management frameworks for efficient energy utilization in a green and sustainable way [4–6]. Besides the harvesting and utilization of renewable energies, green innovations are being popular in recent research perspectives [5]. Green innovations are considered to be potentially enough to substantially reduce the carbon mitigation cost by commissioning economic energy efficient technologies [7]. Solar energy is one of the best easily available options to mitigate future energy demands with an unending energy supply, ease in availability, and a non-polluting source of energy [8]. However, a gap between the energy demand and supply still remains due to the inconsistent and spasmodic way of solar radiation [9–11]. Therefore, suitable thermal energy storage (TES) systems are essential for solar thermal systems to counteract the incongruities between energy demands and supplies.

Phase change materials (PCMs) as thermal energy storage systems are the most potential materials for harvesting and storing capabilities of solar thermal energy with the efficiency of releasing the stowed energy at the time of utilization [12]. Superior thermal energy storage capability, simplicity in fabrication and accomplishment into systems, cost-effective, and commendable temperature-based pertinency are the characteristics of the PCMs which make them potential for TES applications [13]. A considerable amount of research work on PCMs has been conducted for their applications in different sectors viz. building energy management [14,15], agricultural greenhouse [16], biosensors [17–19], heat-barrier textiles [20,21], photovoltaic thermal management [22,23], solar water heaters [24,25], solar thermal power production [26,27], vaccine cold chain transportations [28–30], etc. However, the use of PCMs for real applications is restricted because of their limited thermal conductivity, leakage during phase transformations, high supercooling, and corrosiveness. Therefore, suitable shape stabilization of the PCMs with green and

sustainable materials is crucial for their mass production and actual applications as TES materials.

Applications of solid porous materials with lower density, superior specific area, and a broad range of properties would be suitable for the shape stabilization of PCMs. Contemplating that, biochars are the perfect candidates and can be utilized as green, sustainable, and economic materials for the shape stabilization of PCMs [3,12,31–33]. Biochar is considered as an incipient smart material for their superior properties viz. enormous porosity, extraordinary surface area, low density, greater chemical stability, lower thermal conductivity, and poor flammability [33–35]. Moreover, the presence of active functional groups (viz. -COO^-, -OH^-, –CO, -R-OH, $-NH_2$) on the biochar surfaces make them more potential for various applications. Owing to their superior properties, biochars are widely used for different applications viz. dye removal [36], catalysis [37], biogas purification [38], sediment remediation [39], wastewater treatment [40], agriculture [41], feed supplement for animal [42], restitution of toxic metals in soil and water [42], CO_2 capture [43] etc. The modern advancements have also proved the effectiveness of biochars as building materials as it has thermal insulation properties. Besides, biochars can improve the air quality by soaking moisture as well as acting as carbon sinks. Using biochars in building's envelope can also ensure the prevention of CO_2 re-entering into the atmosphere as well as the entrapment of the same [34,44,45].

In recent times, studies are initiated to exploit biochars for the effective shape stabilizations of PCMs for suitable thermal energy storage applications [3,33]. Phoenix leaf biochar has been reported to shape stabilize paraffin, stearic acid, and polyethylene glycol, and the encapsulation efficiencies are reported to be 49.14, 57.62, and 46.84%, respectively [3]. Neem wood biochar has been reported by Goud et al. [1] to shape stabilize myristyl alcohol and the study shows that 24% biochar can completely fill the PCM into pores. Atinafu et al. [12] have reported biochars from miscanthus straw, oilseed rape, and sewage sludge feedstock to shape stabilize 1-dodecanol and n-dodecane PCMs. Oilseed rape biochar has shown a loading capacity of 71.6% for dodecane and 71.5% for 1-dodecanol with melting enthalpy values of 90.5 and 73.6 kJ/kg, respectively. Lemon peel biochar with a surface area of 55.18 m^2/g has been reported to shape stabilize heptadecane [46]. In another report, Hekimoğlu et al. have reported walnut shell biochar to shape stabilize methyl palmitate with encapsulation efficiency (E%) of 42.39% [47]. Orange peel biochar shape stabilized myristic acid has been reported to have a maximum encapsulation ratio of 39.6% at 4:1 PCM/biochar ratio [33]. Wan et al. have reported pinecone biochar for the form stabilizing of palmitic acid [48].

However, the quality of the biochar and its surface functionality depends on the source of the biomass and its synthesis procedure. Besides, the reported studies on the synthesis of composite PCMs by shape stabilization with biochar are meager as well as most of the reported biochar synthesis have been carried out after chemical activation of the biomass. In this present study, biochars have been synthesized by pyrolyzing in oxygen-restricted environments, without any chemical treatment of the biomasses. Moreover, the understanding of the pore structures on the shape-stabilizing capabilities of the biochar has not been adequately attained. Therefore, the present study has been focused on understanding the effect of pore structures of the biochars on the shape stabilization of PCMs. Bamboo biochar has been synthesized in laboratory and compared with commercially available biochar for shape stabilization of paraffin. Paraffin is vacuum impregnated into those biochars to synthesize biochar PCM composites, and the thermal stability with TES performances are assessed for their apposite applications. The morphologies and structures of as received biochars are examined by SEM, BET, and FTIR. Further, the morphologies and chemical compatibilities of the biochar PCM composites are evaluated by SEM and FTIR. Thermal stability and heat storage efficiencies are assessed using TG-DTA and DSC as well as the resistance against leakage has been performed at room temperature and an elevated temperature beyond the melting point of paraffin.

2. Materials and methods

2.1. Materials

Paraffin (melting point 56–58 °C) is used in this study as PCM and has been procured from Daejung Chemicals, South Korea. Two different biochars have been used for the form stabilization of paraffin. One biochar has been synthesized from the bamboo (*Bambusa vulgaris*) stem collected from Lanchang, Pahang, Malaysia. Another softwood eco-biochar has been procured from K-Agro, Daegu, South Korea. Both the biochars are synthesized directly from the raw materials by pyrolysis at 500 °C, in a restricted oxygen environment and no chemical treatments are carried out prior to the pyrolysis. The collected biochars have been ground and sieved (50 mesh size) to get biochar powders with uniform-sized particles. Biochars originated from bamboo stems and K-Agro company are designated as BA and EB, respectively.

2.2. Biochar-PCM composite synthesis

The phase change composites have been synthesized by vacuum permeation of paraffin into biochars. Before commencing the permeation, the biochars have been kept inside an oven at 100 °C for 12 h to completely remove the trapped moisture, followed by inside a vacuum desiccator overnight to remove the adsorbed gases from the surfaces, pores, and channels. To permeate paraffin into the biochars, 10 g of biochars have been separately mixed with 3 different contents of paraffin, in the ratios of 1:1, 1:2, and 1:3. The biochar to paraffin ratios and their respective nomenclatures are mentioned in Table 1. The permeation method of PCM into biochars has been schematically presented in Fig. 1. For the permeation of paraffin into biochars, the mixture of those two has been taken into an Erlenmeyer flask with side arm, and the flask has been kept on an automatic hotplate magnetic stirrer after connecting the side arm with a vacuum pump (Fig. 1). The temperature and stirring are maintained at 70 °C and 1000 rpm for 4 h. During the permeation procedure, a −0.1 MPa vacuum has been maintained and after the permeation, the excess PCM has been removed from the mixture by vacuum filtration on a filter paper.

2.3. Characterizations

The as-received biochars, paraffin, and the biochar PCM composites are undertaken for attenuated total reflectance-Fourier-transform infrared (ATR-FTIR) spectroscopy (Model: Nicolet IS50, Brand: Thermofisher scientific, United States of America) analysis to understand the chemical coherency between the PCM and shape stabilizing biochars. The morphology of the as-received biochars and biochar PCM composites are examined by a field emission scanning electron microscope (FE-SEM) (Model: S-4800, Brand: Hitachi Japan). The nature of the pore structures and specific surface areas of the biochars are characterized by Brunauer, Emmett, Teller (BET) adsorption isotherm analyzer (Model: 3Flex 5.01, Brand: Micromeritics Georgia, United States of America). The BET analyses are carried out at a relative pressure range of 0–1.0 at 77 K after a degassing period of more than 12 h. A differential scanning calorimeter (DSC) (Model: Q 20, Brand: TA instruments) has been employed to understand the phase transition behavior of pure paraffin and PCM composites. All the DSC scans are carried out at a heating rate of 10 °C/min with continuous purging of Ar gas. The same DSC instrument is used for thermal cycle tests at a heating rate of 20 °C/min. Thermal stability in terms of thermogravimetry of pure paraffin and PCM composites has been examined at a temperature range of 30–500 °C, by simultaneous thermogravimetric/differential thermal analyzer (STA) (Model: STA 6000, Brand: PerkinElmer, United States of America) at 10 °C/min heating rate. Prior to the thermal characterizations, both the instruments have been calibrated for temperature and enthalpy values, using standard zinc. The leakage tests of the PCM composites are done on Whatman filter paper (Grade: 5C, Brand: Advantec, Japan) by keeping on a hot plate (Model: MS300HS, Brand: Mtops, Korea) at ambient temperature (25 ± 2 °C) and 80 °C.

3. Results and discussion

3.1. FTIR spectroscopy

To understand the chemical compatibility among the PCM and the shape-stabilizing materials, FTIR analyses are carried out and the FTIR spectra of the PCMs with two different shape-stabilizing materials are presented in Fig. 2. (a) and (b). Both the FTIR plots are highlighted with two different colours where the yellow highlighted colour corresponds to the absorption peaks contributed from paraffin and the green highlighted colour corresponds to the absorption peaks from biochars. For both the as-received biochar samples, the major absorption peaks are found at 797, 1000, 1237, 1377, and 1580 cm^{-1}. The absorption peaks at 797 cm^{-1} correspond to the C–H bending vibrations [31]. The absorption peaks at 1000 cm^{-1} can be due to the stretching of C–O–C, present in the lignin or stretching of Si–O–Si [49,50]. The aliphatic C–H stretching vibrations in the biochar samples have resulted into the appearance of absorption peaks at 1377 cm^{-1} [51]. The C=O stretching as well as aromatic C=C vibrations have resulted into the appearance of the peaks at 1580 cm^{-1} [52,53].

Below 3000 cm^{-1}, many major peaks have appeared due to the presence of paraffin in the biochar shape stabilized PCM composites. The major intense peaks at 2956 and 2916 cm^{-1} are attributed to the asymmetric stretching of $-CH_3$ and $-CH_2$ groups, respectively. The symmetric stretching of the same groups have resulted into the appearance of absorption peaks at 2873 and 2848 cm^{-1} [54]. Asymmetric in-plane deformations of $-CH_3$ groups as well as in-plane deformation of $-CH_2$ groups have resulted into the occurrence of the peak at 1471 cm^{-1} [55,56]. In plane symmetric deformations of $-CH_3$ groups have resulted into the absorption peak at 1378 cm^{-1} [13]. The absorption peaks appeared at 719 cm^{-1} may be attributed to the $-CH_2$ rocking vibrations [57].

The FTIR analysis of both the biochars shape stabilized PCMs clearly indicates the difference between the frame and core materials. No evidence is found for other functional groups for the new phase formation which implies that there is nothing except the physical interactions between the shape-stabilized materials and PCM.

Table 1 – Biochar to paraffin ratios for synthesizing shape stabilized PCMs.

Sample ID	Biochar	Biochar to paraffin ratio
1-1 PREB	Eco-biochar	1:1
1-2 PREB		1:2
1-3 PREB		1:3
1-1 PRBA	Bamboo biochar	1:1
1-2 PRBA		1:2
1-3 PRBA		1:3

3.2. Morphology and structure of biochars

The morphology of the as-received biochars is verified by FE-SEM (Fig. 3 a, b). The statistics of the pore diameter distribution measured from the SEM images have been presented in Fig. 3c and d for EB and BA, respectively. It can be evidenced from the SEM micrographs that the EB sample (Fig. 3a) is having bigger size pores open to the surface than BA biochar (Fig. 3b) samples. Channel-like morphologies of both the biochars are seen from the FE-SEM micrographs. These channels and pores opened to the surfaces confirm their capability of accommodating PCMs. High structural stability of the PCMs can be provided by these pores and channels when PCMs are incorporated into them; further ensures about higher thermal stability for superior thermal energy storage capability.

The biochar surface properties such as surface area, pore volume, and pore size distribution of both the EB and BA biochars are scrutinized with the N_2 adsorption-desorption method by a BET analyzer. The obtained data of the N_2 adsorption-desorption isotherms of the as-received EB and BA biochars are presented in Fig. 4a and b, respectively. The pore size distribution plots of the same are shown in Fig. 4c and d, respectively. Adsorption capacities of 22.37 and 4.70 cm^3/g at $P/P_0 = 0.99$ are found for EB and BA biochars, respectively. At the ranges of lower relative pressure ($P/P_0 = 0.02$), the N_2 adsorption is almost 4 times higher (8.37 cm^3/g) in EB sample, in comparison to BA sample (2.12 cm^3/g). In accordance with the IUPAC classification, the N_2 adsorption-desorption isotherms of the EB sample can be classified as type IV, indicating

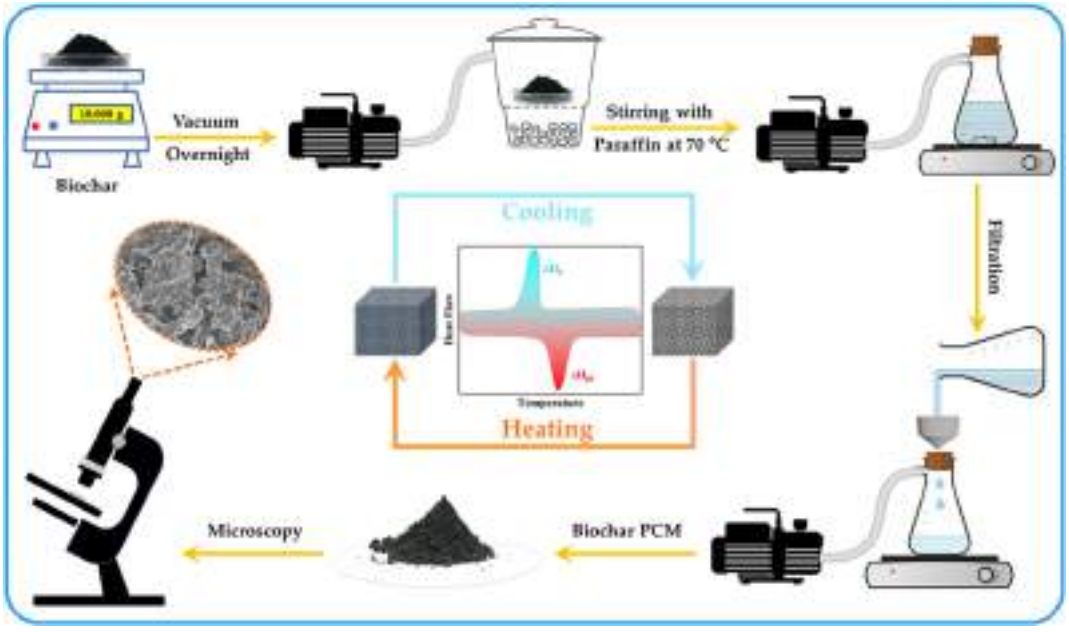

Fig. 1 – Synthesis procedure of the biochar composite PCMs via vacuum permeation.

the micromesoporous adsorption nature. Initially, at a lower relative pressure range, the adsorption isotherm upsurges rapidly in a convex way. At the elevated P/P_0, adsorption isotherm again sharply increases. As soon as the saturation pressure is attained, hysteresis back loop starts, owing to the coalescence of capillary of the porous biochar. Subsequently, when the mesoporous capillary coalescence is completed, the adsorption isotherm further starts to rise. This observation indicates the presence of larger diameter pores or a strong molecular interaction with an adsorbent to result in multimolecular layer adsorption. Hence, a distinctive capillary coalescence phenomenon with multilayer adsorption indicates a type IV isotherm, and the biochar pores are having a combination of micro and mesopores with narrow fissure pores [58–60].

The adsorption characteristic of BA sample seems to be a type I(b) adsorption curve where at the relatively lower pressure range, the adsorption has a sharp upsurge due to the micropore filling. Subsequent to that, at relatively higher pressure, it seems to be multilayer adsorption and capillary condensation. This result infers the presence of both micropores and mesopores in the BA biochar sample [33,61].

The single point surface areas at $P/P_0 = 0.29$ for EB and BA have been obtained 31.6870 m^2/g and 7.3794 m^2/g, respectively. The surface area obtained through BET method is 41.1676 and 9.7213 m^2/g for EB and BA, respectively. The

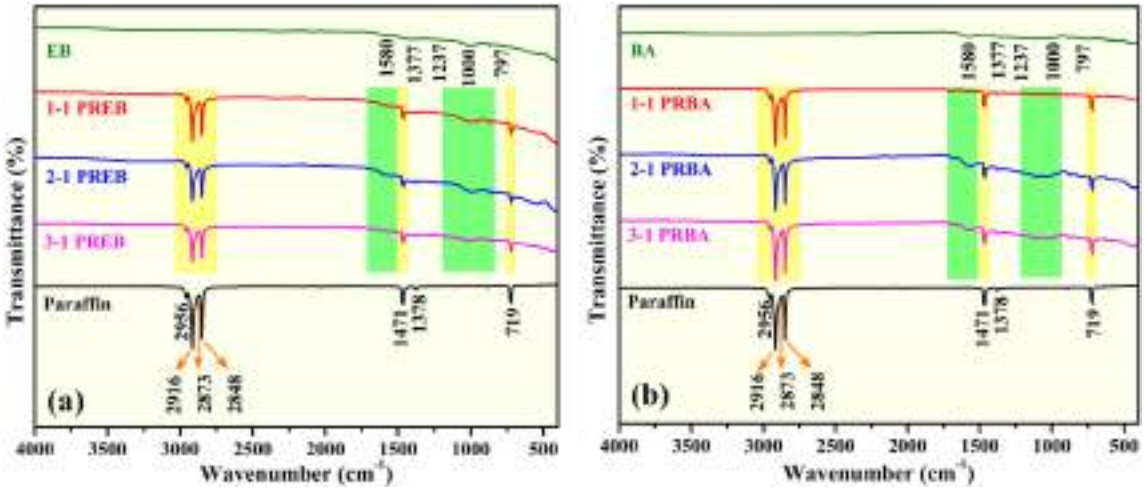

Fig. 2 – FTIR spectra of PREB (a) and PRBA (b) samples with paraffin and as received biochars.

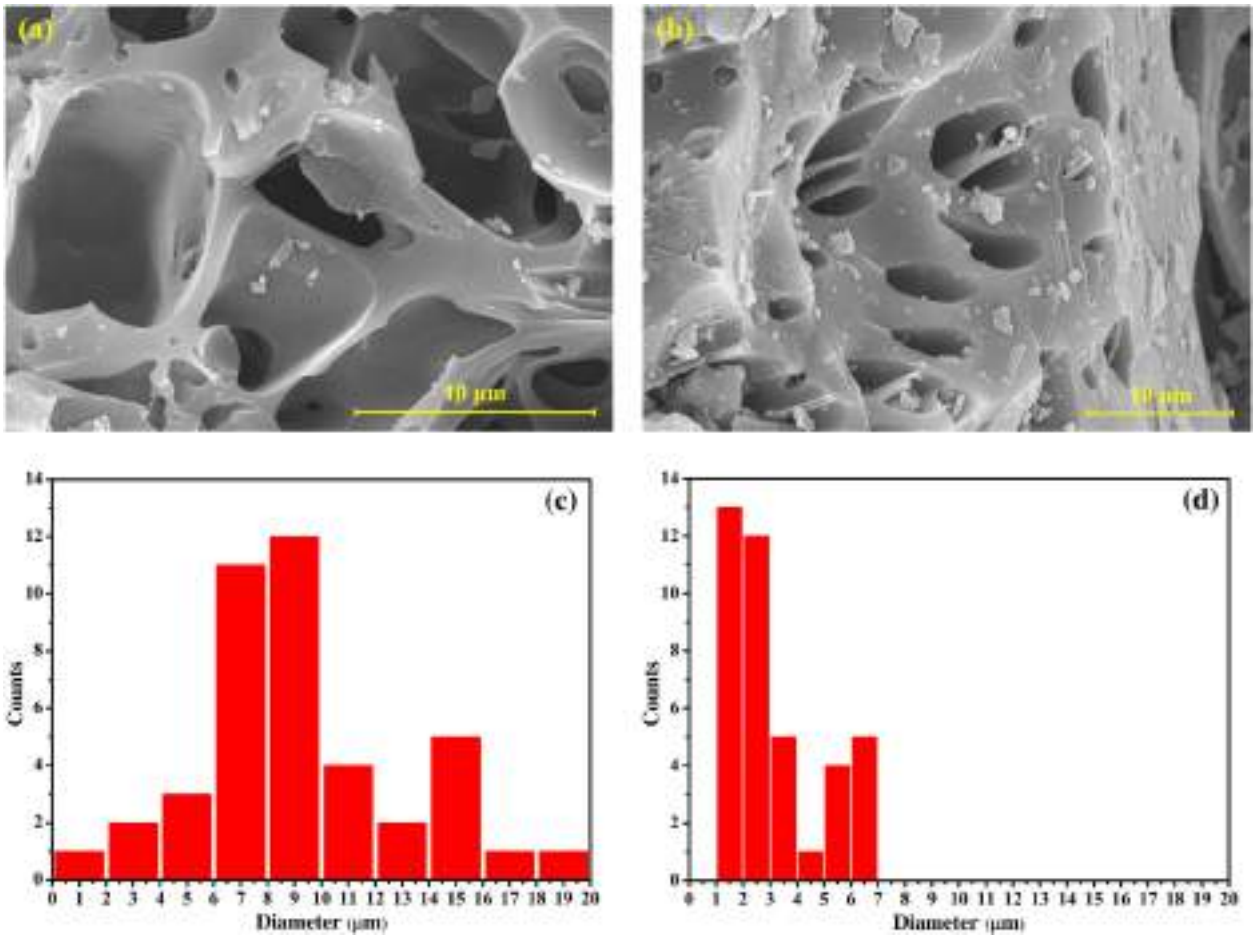

Fig. 3 – SEM micrograph of EB (a), BA (b). Statistics of the pore size distribution and the mean pore diameter of EB (c), BA (d).

adsorption average pore diameters are also obtained by Barrett- Joyner-Halenda (BJH) model, and the plots are presented in Fig. 4c and d. The values of adsorption average pore diameters are found to be 18.336 and 14.095 Å for EB and BA, respectively. Therefore, from the N_2 adsorption-desorption isotherms, it can be realized that the surface area of BA is almost 4 times smaller than EB as well as adsorption average pore diameter is also smaller in BA.

3.3. *Microscopy of shape-stabilized PCM composites*

The shape-stabilized biochar composites are examined under FE-SEM and the micrographs are presented in Fig. 5(a–f). The SEM of the as-received biochars have shown distinct pores and channels in Fig. 3(a and b). However, the composite PCMs demonstrate that the pores and channels are filled with paraffin. For 1-1 PREB (Fig. 5a) and 1-1 PRBA (Fig. 5d) samples, still few unfilled pores are visible (marked with yellow circles), due to the inadequate amount of PCM. The detectable unfilled pores are very less in 1–2 PREB sample (Fig. 5b) and for 1–2 PRBA sample (Fig. 5e). This is attributed to the availability of a higher amount of paraffin for accommodating into the pores and channels of the biochars. However, for PCM composites with 1:3 biochar to paraffin ratios (Fig. 5c and f), the unfilled pores are scarcely detectable. Therefore, it can be realized from the SEM micrographs that 1:3 biochar to paraffin ratio is optimum to fill the pores and channels of the EB and BA biochars. Similar observations have been seen in the TGA and DSC data that beyond the critical content of 1:3 biochar to paraffin, there are no changes in the thermal data. Hence, the data of those PCM composites with higher biochar to PCM have not been considered in this paper. From the SEM observations, it can be realized that both the biochars can accommodate PCMs, 3 times of their mass, into their pores and channels.

3.4. *Evaluation of thermal stability*

The thermal stability of the PCM is a crucial parameter before their real applications. Decomposition resistance against temperature of the PREB and PRBA composite PCMs are evaluated and compared with pure paraffin by thermogravimetric analysis; thermograms are presented in Fig. 6a and c, respectively. The respective differential thermogravimetric (DTG) spectra of PREB and PRBA composite PCMs are presented in Fig. 6b and d. From both the TGA and DTG plots, it can be seen that 100% weight loss without resulting residue has occurred for pure paraffin, as expected. However, the

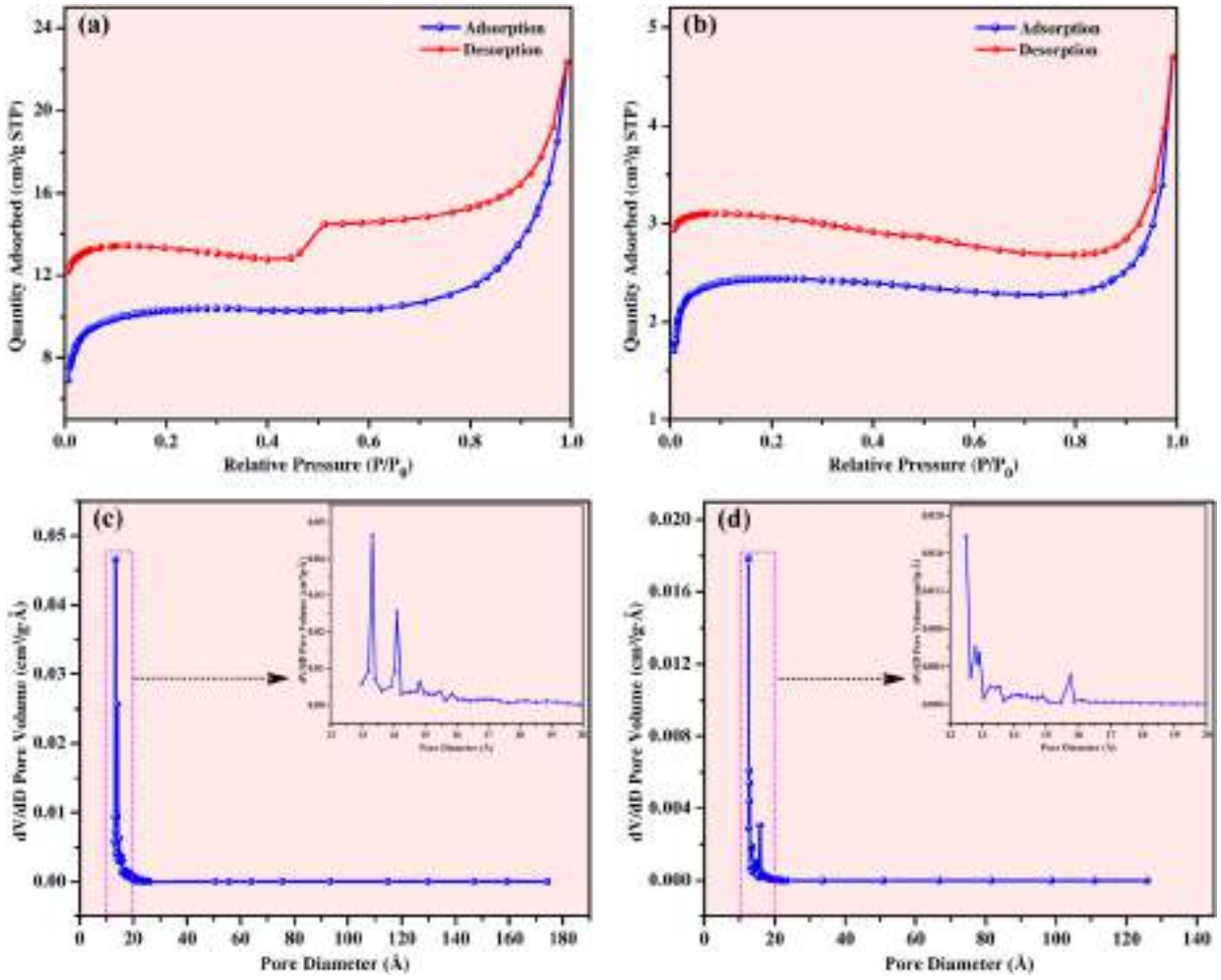

Fig. 4 – N_2 adsorption-desorption isotherms (at 77K) of EB (a), BA (b), and pore size distribution (BJH method) of the as-synthesized EB (c) and BA (d) biochars.

weight losses are more for PREB samples as the pore sizes are bigger in case of EB biochar than BA biochar. Therefore, the accommodability of PCMs into biochar pores and channels is more for EB biochar than the other one. The weight losses are found 42.79, 47.64, and 57.48% for 1-1, 1–2, and 1–3 PREB samples whereas, the same are found to be 33.10, 40.53, and 45.08% for 1-1, 1–2, and 1–3 PRBA samples, respectively. Therefore, PRBA composite PCMs have shown lesser decomposition at elevated temperatures than PREB composite PCMs. However, for the biochar PCM composites, the decomposition onset temperatures have been shifted towards higher temperatures in comparison to paraffin. The onset of decomposition temperature for paraffin is found ~220 °C whereas the same are found to be 236.39 °C and 240.74 °C for 1–3 PREB and 1–3 PRBA samples, respectively. This is due to the surface functionalities, capillary actions, space confinement effects, and other physical factors which are demonstrated in Fig. 10. Though the heat transfer capability and conductivity of the shape-stabilizing materials influence the decomposition onset [62], interactions between the PCM molecules and biochar surface play a significant role to elevate the decomposition onset [32,33,63]. Those physical factors of biochar surfaces prevent the PCMs in core from easy discharge, vaporization, and decomposition. Moreover, the higher thermal stabilities and decomposition onset temperatures demonstrated by PRBA samples than PREB samples are due to the smaller pore size i.e., higher effective surface areas. The TGA and DTG results demonstrate that the synthesized biochar composite PCMs would not go for thermal degradation at an operating temperature for TES applications viz. electronic applications, waste heat recovery, absorption cooling, solar heating etc. [48,64]. PCM permeated biochar composites can provide an uninterrupted heat source in solar absorption cooling and further ensures the recyclability and reusability of the biochars which in turn reduces the environmental contaminants.

3.5. *Evaluation of heat storage capability*

Evaluation of heat storage capability is the most important parameter for PCM materials for their applications as TES material. All the synthesized biochar PCMs and pure paraffin have been evaluated by DSC to understand their heat storage and release capabilities. The DSC thermograms of melting and

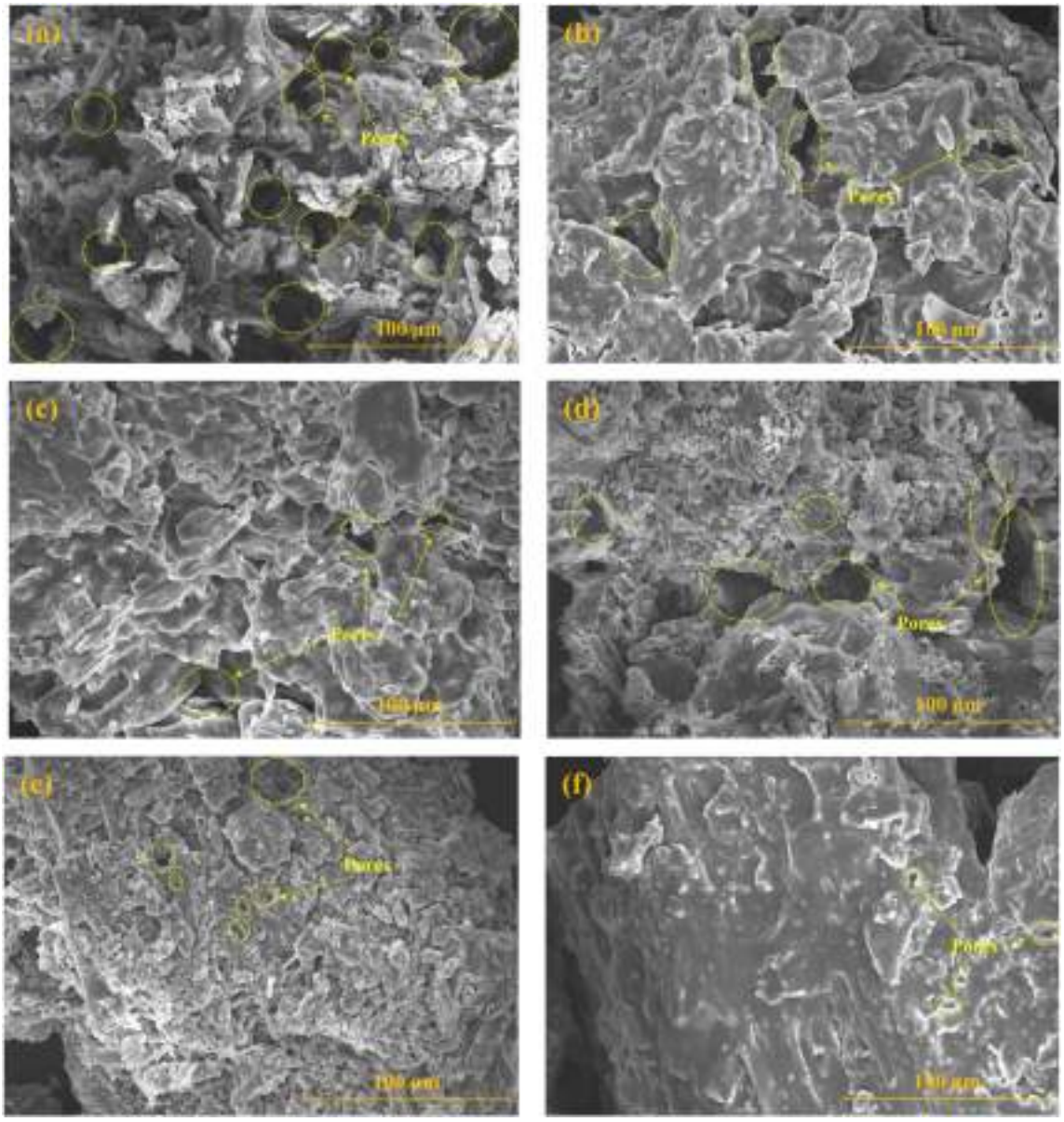

Fig. 5 – SEM micrographs of (a) 1–1 PREB, (b) 1–2 PREB, (c) 1–3 PREB, (d) 1–1 PRBA, (e) 1–2 PRBA, and (f) 1–3 PRBA biochar PCM composites.

solidification events are presented separately in Fig. 7a and b, respectively. Thermal data viz. melting temperature (T_m), solidification temperature (T_s), melting enthalpy (ΔH_m), and solidification enthalpy (ΔH_s) obtained from DSC curves are presented in Table 2. Melting (180.78 J/g) and solidification (176.16 J/g) enthalpies are found maximum for pure paraffin as there is no shape-stabilizing materials. However, for both biochar PCM composite series, 1–3 biochar to PCM ratios have shown the highest enthalpy values. It can be evidenced from the enthalpy values that the values are increased in a consistent manner with increasing the PCM loading into the biochars. However, the enthalpy values are less in PRBA samples in comparison to PREB samples. It is owing to the higher pore size and surface area which leads to the permeation of higher PCM inside EB biochar. Therefore, the highest melting and solidification enthalpies are found to be 96.71 and 94.97 J/g for 1–3 PREB sample whereas the same are found to be 77.78 and 75.06 J/g for 1–3 PRBA sample (Table 2). In case of T_m, it is found to be 58.62 °C for paraffin. Though the T_m are slightly decreased compared to paraffin for PREB samples, T_m has been increased for 1-1 PREB to 1–3 PREB. However, the increment in T_m for 1–2 PREB to 1–3 PREB is negligible. Besides, a prominent and obvious increasing trend in T_m is found in 1-1 PRBA to 1–3 PRBA samples. The T_m has increased from 58.36 °C to 59.02 °C from 1–1 PRBA to 1–3 PRBA samples. Similar observations are found for solidification temperatures also. The T_s of biochar PCMs have been lowered in comparison to paraffin as well with increasing content of paraffin into BA, the T_s has been reduced in a clear trend. However, for PREB samples, no such obvious trend is found for T_s. The T_m and T_s

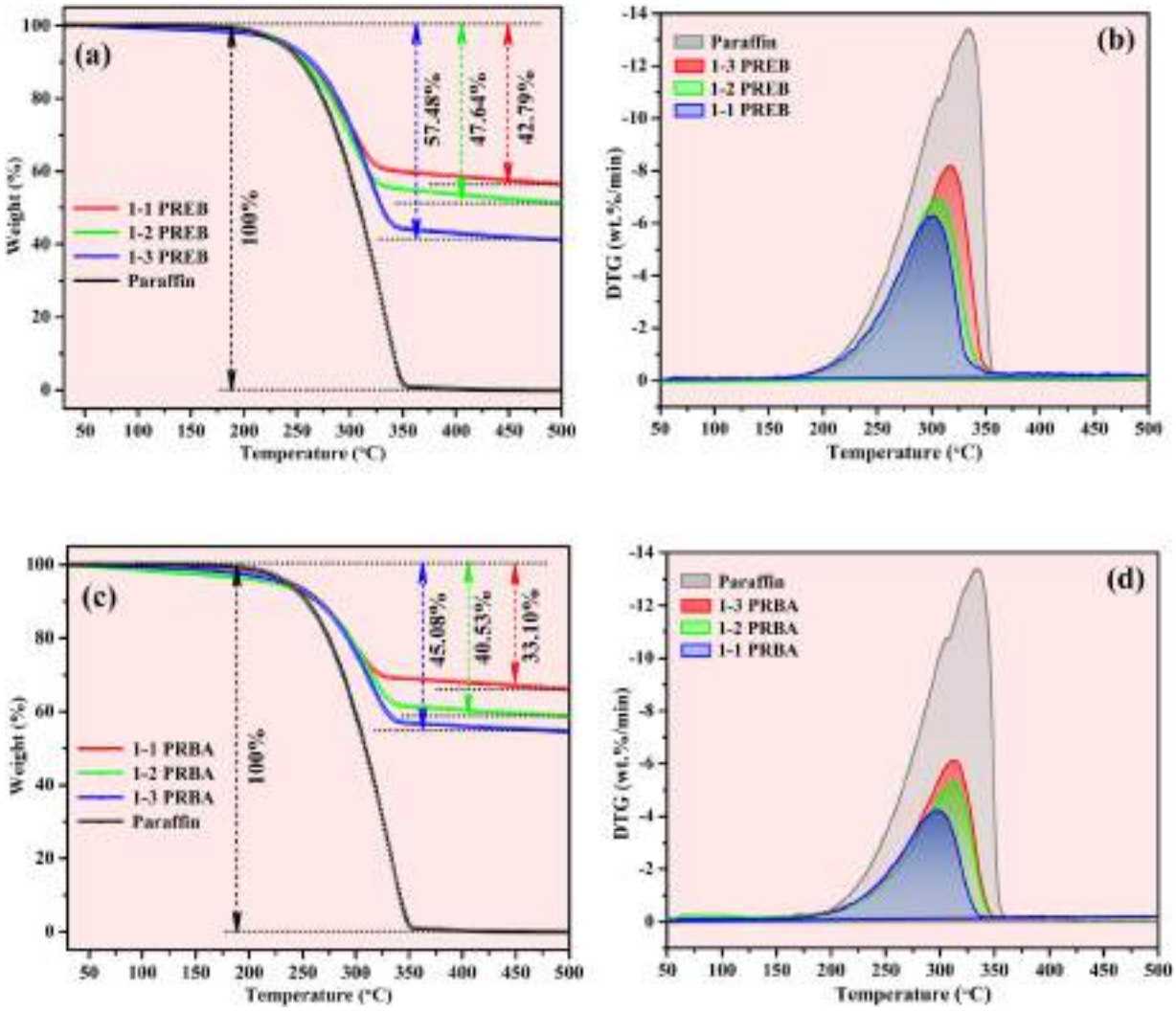

Fig. 6 – TGA (a), (c) and DTG (b), (d) plots of PREB and PRBA samples.

are influenced by the pore sizes and surface areas, space confinement effects, surface tension, van der Waals force, capillary action, and interactions with the functional groups present on the biochar surfaces [delineated in Fig. 10] [3,32,33,63,65]. However, in case of BA, the pore size is smaller in comparison to EB biochar, therefore, the effective surface functionalities are more on PCM, inside BA biochar which ultimately results in elevating the melting and lowering the solidification temperatures. Therefore, clear trends in increasing in T_m and decreasing in T_s have been manifested by the PRBA samples. Generally, biochars are highly porous with adequate surface area, superior chemical stability, lower in density, poor flammability and thermal conductivity [34,35]. For these physical and chemical properties, biochars can be exploited for good thermal insulation in addition with thermal energy storage applications with PCMs.

Moreover, to estimate the thermal performances, encapsulation efficiency (EE%) and encapsulation ratio (ER%) of the synthesized biochar PCM composites are calculated from the obtained ΔH_m and ΔH_s values, by using the following equations [13,66,67]:

$$EE\% = \frac{\left(\Delta H_{m,\ Composite\ PCM} + \Delta H_{s,\ Composite\ PCM}\right)}{\left(\Delta H_{m,\ Paraffin} + \Delta H_{s,\ Paraffin}\right)} \times 100 \quad (1)$$

$$ER\% = \frac{\Delta H_{m,\ Composite\ PCM}}{\Delta H_{m,\ Paraffin}} \times 100 \quad (2)$$

where, melting and solidification enthalpy values of biochar PCM composites and paraffin are denoted by the $\Delta H_{m,\ Composite\ PCM}$, $\Delta H_{s,\ Composite\ PCM}$, $\Delta H_{m,\ Paraffin}$, $\Delta H_{s,\ Paraffin}$, respectively.

The deduced EE% and ER% are presented in Table 2. It is evidenced for both the PCM composite series, the highest EE% and ER% have been found for 1:3 biochar to paraffin ratios, as the PCM contents are highest for those ratios. The highest EE% and ER% found for 1–3 PREB are 53.70 and 53.49% whereas, the same are found to be 42.82 and 43.02% for 1–3 PRBA, respectively. The ER% of 38.58% has been reported for palmitic acid into Pinus fruit biochar in a 6.5:3.5 ratio [48]. Polyethylene glycol into almond shell biochar in 3.5:1.5 has been reported to have 43.76% of ER% [68]. The introduction of myristic acid in orange peel biochar in 4:1 ratio has resulted in ER% at 39.6% [33]. Eicosane to wheat straw biochar in 2:1 ratio has been

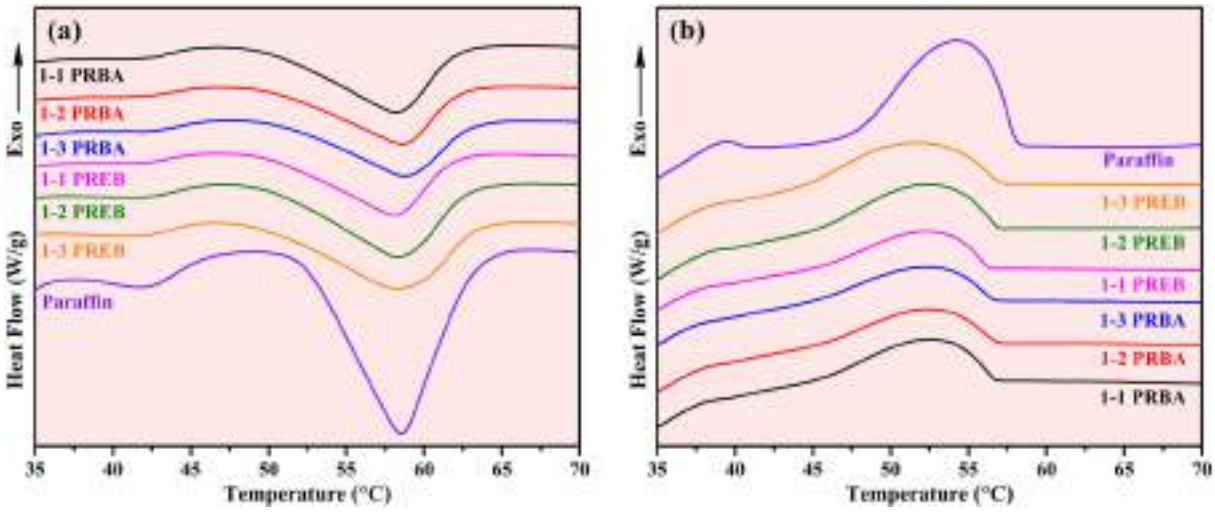

Fig. 7 – DSC plots of (a) melting and (b) solidification of paraffin, PREB, and PRBA PCMs.

reported by Atinafu et al. to have 37.1 ER%. ER% of 36.0 and 29.3% have been reported for 2:1 n-dodecane and 1-dodecanol into sewage sludge feedstock, respectively [12]. The highest ER of 32.66% has been reported for dodecanoic acid into pinus fruit biochar in 4:1 ratio [32]. Oilseed rape biochar has been used as shape stabilizing material for 1-dodecanol and n-dodecane in PCM to biochar ratio of 2:1 and the ER% have been reported to be 60.2 and 29.3%, respectively [12]. Palm wax into rice husk biochar has been reported with an encapsulation ratio of 50.1% [31]. Hekimoğlu et al. have reported a value of 51.6 ER% for hazelnut wood biochar shape stabilized capric acid PCM composite [69].

The obtained thermal data from DSC show the melting and solidification temperature ranges of these synthesized biochar PCM composites between 58-59 °C and 56.68–57.09 °C. These PCM composites also reveal the capabilities of adequate heat charging and discharging. Therefore, these biochar-based PCM composites can be utilized in different fields viz. solar energy utilization, agricultural technology, building energy conservation, cold chain temperature control, and solar refrigeration purposes [65]. Moreover, copious availability of biochar resources and ease of biochar processing ensure the cost-effectiveness of biochar-based PCM synthesis with superior thermal properties and environmental remediations.

3.6. *Thermal cycle endurance*

The congruency in heat charging and discharging is another important parameter to be accounted for good phase change materials for their real-life applications. To examine the consistency in latent heat storage and release, 1–3 PREB and 1–3 PRBA samples are undertaken for 200 heating and cooling cycles by DSC at 20 °C/min, in isochronal mode with an isothermal holding of 3 min, prior to each heating and cooling segments (Fig. 8 c-d). The 1st and each 20th cycles of heating and cooling thermograms of 1–3 PREB and 1–3 PRBA samples are displayed in Fig. 8a and b, respectively. It can be depicted from the DSC thermograms (Fig. 8a and b) that both the samples provide unaltered melting and solidification enthalpies even after 200th cycles of heating and cooling. For a better understanding of the charging and discharging manners of the samples, time vs. heat flow curves are also presented in Fig. 8c and d. From those figures, it can be seen that both the samples complete a thermal cycle in 13 min where a period of 3.5 min is required for each charging and discharging with two isothermal events of 3 min, prior to heating and cooling. For 1–3 PREB, congruent durations of 1.44 and 1.06 min are found up to 200th cycles of heating and cooling, respectively. Similar consistent charging and discharging

Table 2 – Melting, solidification and encapsulation parameters of pure paraffin and biochar PCM composites, deduced from DSC thermograms.

Sample ID	$T_{m\ (onset)}$ (°C)	T_m (°C)	ΔH_m (J/g)	$T_{s\ (onset)}$ (°C)	T_s (°C)	ΔH_s (J/g)	ER%	EE%
Paraffin	52.3	58.62	180.78	58.05	54.27	176.16	–	–
1-1 PREB	50.98	58.08	69.33	56.68	52.17	66.97	38.35	38.19
1-2 PREB	50.72	58.47	80.37	56.87	52.03	77.13	44.46	44.13
1-3 PREB	51.35	58.48	96.71	56.75	51.20	94.97	53.49	53.70
1-1 PRBA	50.53	58.36	49.72	56.73	52.61	47.66	27.50	27.28
1-2 PRBA	51.3	58.65	62.34	56.83	52.46	58.38	34.48	33.82
1-3 PRBA	51.60	59.02	77.78	57.09	52.24	75.06	43.02	42.82

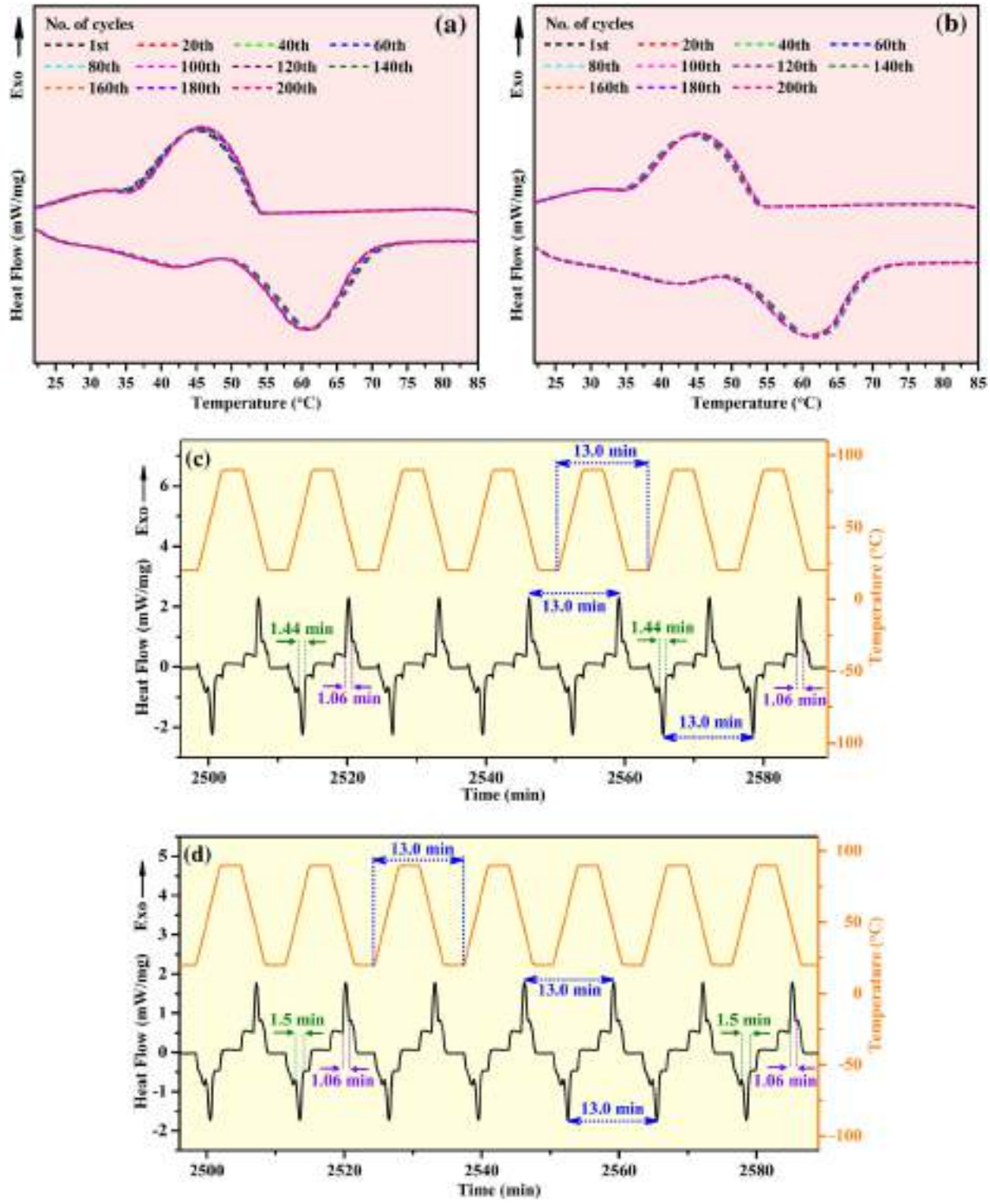

Fig. 8 – 1st and every 20th cycles of heating and cooling (a) 1–3 PREB and (b) 1–3 PRBA. Thermal charging and discharging consistency with time (c) 1–3 PREB and (d) 1–3 PRBA.

durations of 1.5 and 1.06 min are found for 1–3 PRBA sample. An important observation can be seen from the time vs. heat flow plots that both the samples take the same time (1.06 min) for the exothermic events (solidification), though the time required for endothermic events (melting) is higher (1.5 min) for 1–3 PRBA than 1–3 PREB (1.44 min). Similar observations can be realized from the DSC thermograms (Fig. 8a and b) that the endothermic peak is sharper in the case of 1–3 PREB samples. This is due to the smaller pore size (SEM and BET results) which facilitates with higher effective surface area,

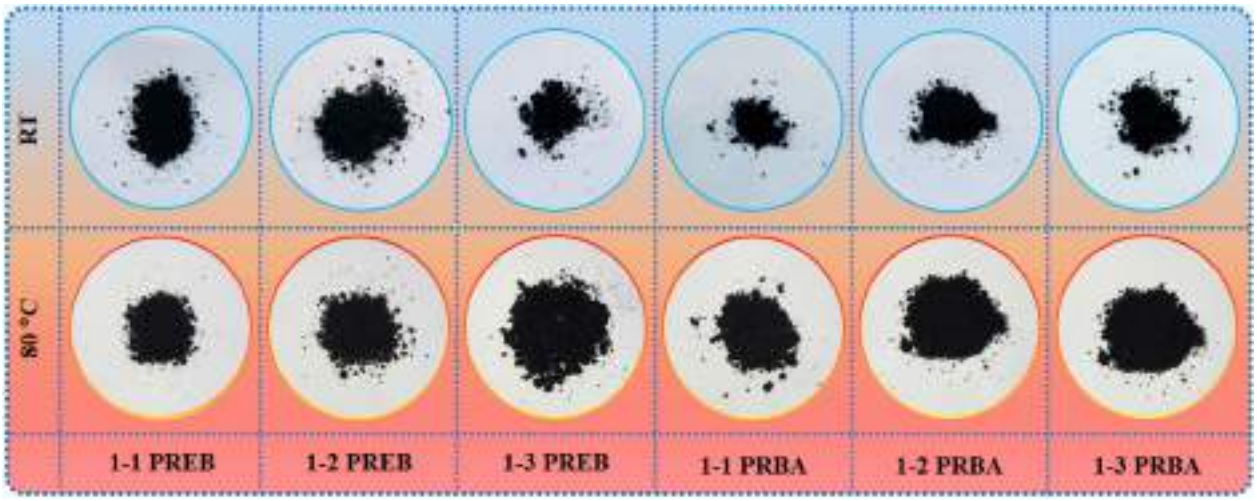

Fig. 9 – Leakage tests of the biochar PCMs at room temperature (RT) and 80 °C.

and superiority in capillary actions in BA and other surface functionalities (Fig. 10) which hinders the melting of PCM inside BA. For both the samples, the congruency in heat charging and discharging is due to the space confinement effects, surface tension, van der Waals force, and capillary action which influence the melting and solidification of paraffin inside the pores and capillaries [32,33]. Consistency in the thermal cycle ensures the samples' suitability as thermal energy storage applications viz. electronic applications, waste heat recovery, absorption cooling, solar heating etc. [64].

3.7. *Leakage assessment*

To understand the extent of shape stabilization of PCM that has been accomplished by the impregnation of them into biochar pores, it is crucial to assess the PCM composite by leakage tests. The biochar PCM composites are taken on Whatman filter papers and have been subjected to keep at room temperature and a temperature (80 °C) higher than the melting point (58 °C) of paraffin, to visually inspect the stain of soaking if the leakages occur. As expected, pure paraffin is melted as soon as the temperature reaches its melting point (58 °C), therefore the photograph of pure paraffin has not been included. However, from the leakage assessment of the biochar PCM composites (Fig. 9), no leakages have been observed for any samples. This leakage test results confirm the successful permeation of paraffin into the channels and pores of both the biochars; further ensuring the shape stability of those PCM composites at an elevated temperature beyond the melting point of paraffin. The surface tension and capillary actions provided by the biochar surfaces and pores prevent the PCM from leakage [70]. Moreover, various functional

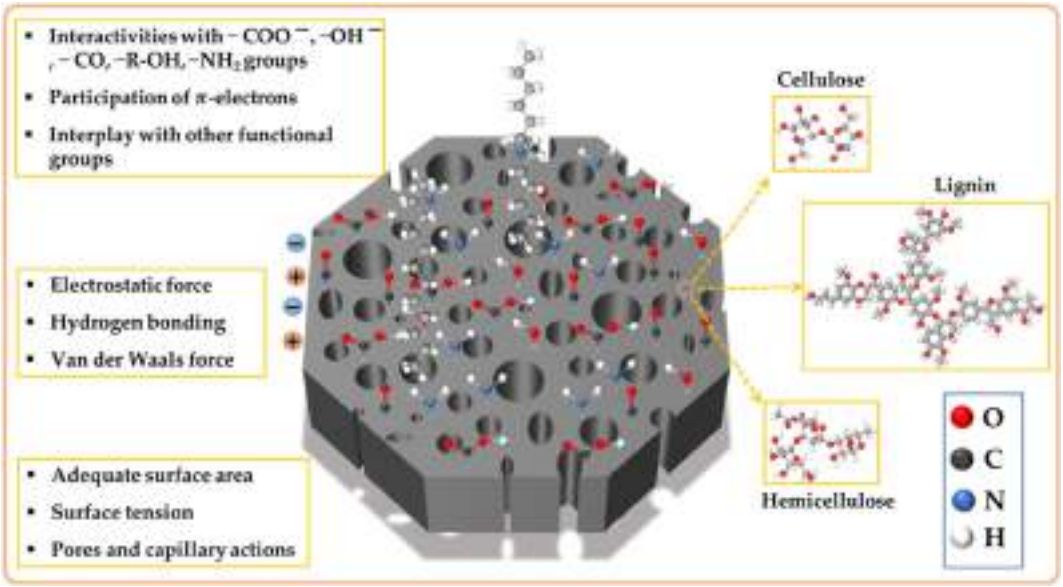

Fig. 10 – Schematic of the surface functionalities of biochar and the interaction between the PCM and biochar surfaces.

groups (viz. -COO^-, -OH^-, −CO, -R-OH, $-NH_2$) present in the biochar surfaces, form hydrogen bonding. Other factors viz. Van der Wall force, π-electron participation, interactions with other functional groups and electrostatic forces (Fig. 10) are responsible for providing shape stability as well as leakage-free performances at elevated temperatures [32,33,62,63,71]. This result ensures the safe and leakage-free performances of the synthesized biochar PCM composites for TES applications.

4. Conclusions

In this present study, a comparative study has been conducted on the biochar PCM composites with commercially available biochar (EB) and bamboo biochar (BA). Paraffin has been permeated into the biochar pores and channels, and stabilities with thermal performances are evaluated for TES applications. From this study, the conclusions can be drawn as following.

(i) From the SEM and N_2 adsorption-desorption analyses, it is found that the EB biochar is having pores with bigger sizes. The EB biochar demonstrates type IV and BA shows type I(b) isotherms. Both biochars are having a combination of micro and mesopores.
(ii) The SEM morphologies of the biochar PCM composites demonstrate that 1:3 biochar to PCM ratio is optimum for both biochar PCM composites for the maximum accommodability of PCM into biochars.
(iii) In comparison to paraffin, the shape-stabilized PCM composites show higher thermal stabilities against decomposition as the onsets of decomposition shift towards higher temperatures. PRBA PCM composites show higher onsets of decomposition than PREB samples, but the weight losses found higher in PREB samples in comparison to PRBA samples.
(iv) Higher melting and solidification enthalpies are found in PREB PCM composites which have resulted in higher encapsulation ratios and efficiencies. However, in case of BA, the pore size is smaller in comparison to EB biochar, therefore, the effective surface functionalities are more on PCM, inside BA biochar which ultimately results increasing in T_m and decreasing in T_s in PRBA samples.
(v) Both samples take the same time (1.06 min) for solidifications, though the time required for melting is higher (1.5 min) for 1−3 PRBA than 1−3 PREB (1.44 min).
(vi) Leakage test results at room temperature and 80 °C (beyond the T_m of paraffin) demonstrate that there are no leakages in the shape stabilized PCM composites even at a quite higher temperature than the T_m of paraffin (58 °C).
(vii) The surface tension and capillary actions provided by the biochar surfaces and pores, prevent the PCM from leakage. Moreover, various functional groups (viz. -COO^-, -OH^-, −CO, -R-OH, $-NH_2$) present in the biochar surfaces, form hydrogen bonding, and other factors viz. Van der Wall forces, π-electron participation, interactions with other functional groups, and electrostatic forces are responsible for the superior performances of the composite PCMs.
(viii) Abundant availability of resources and ease in processing ensure the cost-effectiveness of biochar-based PCM synthesis with superior thermal properties and environmental remediations.

Credit authorship contribution statement

Soumen Mandal: Conceptualization, Methodology, Data curation, Formal analysis, Writing – original draft, review & editing. **Shafiq Ishak:** Conceptualization, Methodology, Data curation, Formal analysis, Writing – review & editing. **Mohd Azreen Mohd Ariffin:** Resources, review. **Dong-Eun Lee:** Supervision, Fund acquisition, Writing – review & editing. **Taejoon Park:** Supervision, Fund acquisition, Writing – review & editing.

Data availability

Data will be made available on request.

Declaration of competing interest

The authors declare that they have no known competing financial interests or personal relationships that could have appeared to influence the work reported in this paper.

Acknowledgements

This work was supported by the National Research Foundation of Korea (NRF) grant funded by the Ministry of Science and ICT (MSIT), Korea (No. NRF-2018R1A5A1025137) and National Research Foundation of Korea (NRF) for Creative Challenge Research Foundation Support Project (No. NRF-2020R1I1A1A01072922).

REFERENCES

[1] Goud M, Raval F. A sustainable biochar-based shape stable composite phase change material for thermal management of a lithium-ion battery system and hybrid neural network modeling for heat flow prediction. J Energy Storage 2022;56:106163.
[2] Nam J, Yun BY, Choi JY, Kim S. Potential of wood as thermal energy storage materials: different characteristics depending on the hierarchical structure and components. Int J Energy Res 2022;46:14926–45.
[3] Lv L, Wang J, Ji M, Zhang Y, Huang S, Cen K, et al. Effect of structural characteristics and surface functional groups of biochar on thermal properties of different organic phase change materials: dominant encapsulation mechanisms. Renew Energy 2022;195:1238–52.
[4] He P, Cao M-S, Cai Y-Z, Shu J-C, Cao W-Q, Yuan J. Self-assembling flexible 2D carbide MXene film with tunable integrated electron migration and group relaxation toward energy storage and green EMI shielding. Carbon 2020;157:80–9.

[5] Sun H, Edziah BK, Sun C, Kporsu AK. Institutional quality, green innovation and energy efficiency. Energy Pol 2019;135:111002.
[6] Ishak S, Mandal S, Lee H-S, Singh JK. pH-controlled synthesis of sustainable lauric acid/SiO2 phase change material for scalable thermal energy storage. Sci Rep 2021;11:1–15.
[7] Popp D. The role of technological change in green growth (No. w18506). National Bureau of Economic Research; 2012.
[8] Ramaraj BK, Kottala RK. Preparation and characterisation of binary eutectic phase change material/activated porous bio char/multi walled carbon nano tubes as composite phase change material. Fullerenes, Nanotub Carbon Nanostruct 2023;31(1):75–89.
[9] Bs J, Ramaraj BK, Kottala RK, Sp S. A complete numerical model for low temperature composite form-stable phase change material slab based on dynamically simplified temperature transforming method. Energy Sources, Part A Recovery, Util Environ Eff 2021:1–26.
[10] Kottala RK, Ramaraj BK, Bs J, Vempally MG, Lakshmanan M. Experimental investigation and neural network modeling of binary eutectic/expanded graphite composites for medium temperature thermal energy storage. Energy Sources, Part A Recovery, Util Environ Eff 2022:1–24.
[11] Ravi Kumar K, Balasubramanian K, Jinshah B, Abhishek N. Experimental analysis and neural network model of MWCNTs enhanced phase change materials. Int J Thermophys 2022;43:1–31.
[12] Atinafu DG, Chang SJ, Kim K-H, Kim S. Tuning surface functionality of standard biochars and the resulting uplift capacity of loading/energy storage for organic phase change materials. Chem Eng J 2020;394:125049.
[13] Mandal S, Ishak S, Singh JK, Lee D-E, Park T. Synthesis and application of paraffin/silica phase change nanocapsules: experimental and numerical approach. J Energy Storage 2022;51:104407.
[14] Liu J, Liu Y, Yang L, Liu T, Zhang C, Dong H. Climatic and seasonal suitability of phase change materials coupled with night ventilation for office buildings in Western China. Renew Energy 2020;147:356–73.
[15] Tyagi V, Buddhi D, Kothari R, Tyagi S. Phase change material (PCM) based thermal management system for cool energy storage application in building: an experimental study. Energy Build 2012;51:248–54.
[16] Marinković M, Nikolić R, Savović J, Gadžurić S, Zsigrai I. Thermochromic complex compounds in phase change materials: possible application in an agricultural greenhouse. Sol Energy Mater Sol Cell 1998;51:401–11.
[17] Miao X, Ling L, Shuai X. Sensitive detection of glucose in human serum with oligonucleotide modified gold nanoparticles by using dynamic light scattering technique. Biosens Bioelectron 2013;41:880–3.
[18] Lin C, Du Y, Wang S, Wang L, Song Y. Glucose oxidase@ Cu-hemin metal-organic framework for colorimetric analysis of glucose. Mater Sci Eng C 2021;118:111511.
[19] Sun Z, Liu H, Wang X. Thermal self-regulatory intelligent biosensor based on carbon-nanotubes-decorated phase-change microcapsules for enhancement of glucose detection. Biosens Bioelectron 2022;195:113586.
[20] Su Y, Zhu W, Tian M, Wang Y, Zhang X, Li J. Intelligent bidirectional thermal regulation of phase change material incorporated in thermal protective clothing. Appl Therm Eng 2020;174:115340.
[21] Krzemińska S, Greszta A, Różański A, Safandowska M, Okrasa M. Effects of heat exposure on the properties and structure of aerogels for protective clothing applications. Microporous Mesoporous Mater 2019;285:43–55.
[22] Browne M, Norton B, McCormack S. Phase change materials for photovoltaic thermal management. Renew Sustain Energy Rev 2015;47:762–82.
[23] Ma T, Yang H, Zhang Y, Lu L, Wang X. Using phase change materials in photovoltaic systems for thermal regulation and electrical efficiency improvement: a review and outlook. Renew Sustain Energy Rev 2015;43:1273–84.
[24] Wu H-y, Li S-t, Shao Y-w, Jin X-z, Qi X-d, Yang J-h, et al. Melamine foam/reduced graphene oxide supported form-stable phase change materials with simultaneous shape memory property and light-to-thermal energy storage capability. Chem Eng J 2020;379:122373.
[25] Fazilati MA, Alemrajabi AA. Phase change material for enhancing solar water heater, an experimental approach. Energy Convers Manag 2013;71:138–45.
[26] Kalidasan B, Pandey A, Shahabuddin S, Samykano M, Thirugnanasambandam M, Saidur R. Phase change materials integrated solar thermal energy systems: global trends and current practices in experimental approaches. J Energy Storage 2020;27:101118.
[27] He M, Yang L, Lin W, Chen J, Mao X, Ma Z. Preparation, thermal characterization and examination of phase change materials (PCMs) enhanced by carbon-based nanoparticles for solar thermal energy storage. J Energy Storage 2019;25:100874.
[28] Sha Y, Hua W, Cao H, Zhang X. Properties and encapsulation forms of phase change material and various types of cold storage box for cold chain logistics: a review. J Energy Storage 2022;55:105426.
[29] Liu L, Zhang X, Xu X, Lin X, Zhao Y, Zou L, et al. Development of low-temperature eutectic phase change material with expanded graphite for vaccine cold chain logistics. Renew Energy 2021;179:2348–58.
[30] Calati M, Hooman K, Mancin S. Thermal Storage based on Phase Change Materials (PCMs) for refrigerated transport and distribution applications along the cold chain: a review. International Journal of Thermofluids 2022;16:100224.
[31] Jeon J, Park JH, Wi S, Yang S, Ok YS, Kim S. Latent heat storage biocomposites of phase change material-biochar as feasible eco-friendly building materials. Environ Res 2019;172:637–48.
[32] Mandal S, Ishak S, Lee D-E, Park T. Optimization of eco-friendly Pinus resinosa biochar-dodecanoic acid phase change composite for the cleaner environment. J Energy Storage 2022;55:105414.
[33] Mandal S, Ishak S, Lee D-E, Park T. Shape-stabilized orange peel/myristic acid phase change materials for efficient thermal energy storage application. Energy Rep 2022;8:9618–28.
[34] Gupta S, Kua HW. Factors determining the potential of biochar as a carbon capturing and sequestering construction material: critical review. J Mater Civ Eng 2017;29:04017086.
[35] Jeon J, Park JH, Wi S, Yang S, Ok YS, Kim S. Characterization of biocomposite using coconut oil impregnated biochar as latent heat storage insulation. Chemosphere 2019;236:124269.
[36] Wu J, Yang J, Feng P, Huang G, Xu C, Lin B. High-efficiency removal of dyes from wastewater by fully recycling litchi peel biochar. Chemosphere 2020;246:125734.
[37] Balajii M, Niju S. Biochar-derived heterogeneous catalysts for biodiesel production. Environ Chem Lett 2019;17:1447–69.
[38] Papurello D, Gandiglio M, Kafashan J, Lanzini A. Biogas purification: a comparison of adsorption performance in d4 siloxane removal between commercial activated carbons and waste wood-derived char using isotherm equations. Processes 2019;7:774.

[39] Yang Y, Ye S, Zhang C, Zeng G, Tan X, Song B, et al. Application of biochar for the remediation of polluted sediments. J Hazard Mater 2021;404:124052.
[40] Wang S, Zhang H, Wang J, Hou H, Du C, Ma P-C, et al. Application of biochar for wastewater treatment, biochar and its application in bioremediation. Springer; 2021. p. 67–90.
[41] Das SK, Ghosh GK, Avasthe R. Application of biochar in agriculture and environment, and its safety issues. Biomass Conversion and Biorefinery 2023;13:1359–69.
[42] Bolan N, Hoang SA, Beiyuan J, Gupta S, Hou D, Karakoti A, et al. Multifunctional applications of biochar beyond carbon storage. Int Mater Rev 2022;67(2):150–200.
[43] Ahmed R, Liu G, Yousaf B, Abbas Q, Ullah H, Ali MU. Recent advances in carbon-based renewable adsorbent for selective carbon dioxide capture and separation-A review. J Clean Prod 2020;242:118409.
[44] Schmidt H-P, Wilson K. 55 uses of biochar. Ithaka J 2012;1:286–9.
[45] Legan M, Gotvajn AŽ, Zupan K. Potential of biochar use in building materials. J Environ Manag 2022;309:114704.
[46] Hekimoğlu G, Sarı A, Arunachalam S, Arslanoğlu H, Gencel O. Porous biochar/heptadecane composite phase change material with leak-proof, high thermal energy storage capacity and enhanced thermal conductivity. Powder Technol 2021;394:1017–25.
[47] Hekimoğlu G, Sarı A, Kar T, Keleş S, Kaygusuz K, Tyagi V, et al. Walnut shell derived bio-carbon/methyl palmitate as novel composite phase change material with enhanced thermal energy storage properties. J Energy Storage 2021;35:102288.
[48] Wan Y-c, Chen Y, Cui Z-x, Ding H, Gao S-f, Han Z, Gao J-k. A promising form-stable phase change material prepared using cost effective pinecone biochar as the matrix of palmitic acid for thermal energy storage. Sci Rep 2019;9:1–10.
[49] Collett C, Mašek O, Razali N, McGregor J. Influence of biochar composition and source material on catalytic performance: the carboxylation of glycerol with CO2 as a case study. Catalysts 2020;10:1067.
[50] Pattnaik D, Kumar S, Bhuyan S, Mishra S. Effect of carbonization temperatures on biochar formation of bamboo leaves. In: IOP conference series: materials science and engineering. IOP Publishing; 2018, 012054.
[51] Wengang L, Fang C, Rong Z, Cuihong C. Biochar-mediated degradation of roxarsone by shewanella oneidensis MR-1. Front Microbiol 2022;13:846228.
[52] Behazin E, Ogunsona E, Rodriguez-Uribe A, Mohanty AK, Misra M, Anyia AO. Mechanical, chemical, and physical properties of wood and perennial grass biochars for possible composite application. Bioresources 2016;11:1334–48.
[53] Li C, Huang Q, Zhang H, Wang Q, Xue R, Guo G, Hu J, et al. Characterization of biochars produced by co-pyrolysis of Hami melon (cantaloupes) straw mixed with polypropylene and their adsorption properties of cadmium. Int J Environ Res Publ Health 2021;18:11413.
[54] Sharifah I, Nurul AT, Khairusshima MN. Thermal modelling and analysis of batik canting design. Procedia Eng 2017;184:326–33.
[55] Ullah R, Ahmad I, Zheng Y. Fourier transform infrared spectroscopy of "bisphenol A". Journal of Spectroscopy 2016;2016:2073613.
[56] Davis R, Mauer LJ. Fourier transform infrared (FT-IR) spectroscopy: a rapid tool for detection and analysis of foodborne pathogenic bacteria. Current research, technology and education topics in applied microbiology and microbial biotechnology 2010;2:1582–94.
[57] Valentini F, Dorigato A, Pegoretti A, Tomasi M, Soraru GD, Biesuz M. Si 3 N 4 nanofelts/paraffin composites as novel thermal energy storage architecture. J Mater Sci 2021;56:1537–50.
[58] Zhu M, Yao J, Dong L, Sun J. Adsorption of naphthalene from aqueous solution onto fatty acid modified walnut shells. Chemosphere 2016;144:1639–45.
[59] Tseng R-L. Mesopore control of high surface area NaOH-activated carbon. J Colloid Interface Sci 2006;303:494–502.
[60] Wang W, Li D, Xiang P, Zheng Y, Zheng Z, Lin X, et al. One-step pyrolysis of nitrogen-containing chemicals and biochar derived from walnut shells to absorb polycyclic aromatic hydrocarbons (PAHs). Int J Mol Sci 2022;23:15193.
[61] Qi L, Tang X, Wang Z, Peng X. Pore characterization of different types of coal from coal and gas outburst disaster sites using low temperature nitrogen adsorption approach. Int J Min Sci Technol 2017;27:371–7.
[62] Atinafu DG, Yun BY, Kim YU, Wi S, Kim S. Introduction of eicosane into biochar derived from softwood and wheat straw: influence of porous structure and surface chemistry. Chem Eng J 2021;415:128887.
[63] Bordoloi U, Das D, Kashyap D, Patwa D, Bora P, Muigai HH, Kalita P. Synthesis and comparative analysis of biochar based form-stable phase change materials for thermal management of buildings. J Energy Storage 2022;55:105801.
[64] Du K, Calautit J, Wang Z, Wu Y, Liu H. A review of the applications of phase change materials in cooling, heating and power generation in different temperature ranges. Appl Energy 2018;220:242–73.
[65] Liang Q, Pan D, Zhang X. Construction and application of biochar-based composite phase change materials. Chem Eng J 2023;453:139441.
[66] Ishak S, Mandal S, Lee H-S, Singh JK. Microencapsulation of stearic acid with SiO2 shell as phase change material for potential energy storage. Sci Rep 2020;10:1–15.
[67] Ishak S, Mandal S, Lee H-S, Singh JK. Effect of core-shell ratio on the thermal energy storage capacity of SiO2 encapsulated lauric acid. J Energy Storage 2021;42:103029.
[68] Chen Y, Cui Z, Ding H, Wan Y, Tang Z, Gao J. Cost-effective biochar produced from agricultural residues and its application for preparation of high performance form-stable phase change material via simple method. Int J Mol Sci 2018;19:3055.
[69] Hekimoğlu G, Sarı A, Kar T, Keleş S, Kaygusuz K, Yıldırım N, et al. Carbonized waste hazelnut wood-based shape-stable composite phase change materials for thermal management implementations. Int J Energy Res 2021;45:10271–84.
[70] Atinafu DG, Yun BY, Yang S, Kim S. Encapsulation of dodecane in gasification biochar for its prolonged thermal/shape stability, reliability, and ambient enthalpy storage. Chem Eng J 2022;437:135407.
[71] Oliveira FR, Patel AK, Jaisi DP, Adhikari S, Lu H, Khanal SK. Environmental application of biochar: current status and perspectives. Bioresour Technol 2017;246:110–22.